

Article

Design of a New Capacitive Load Cross-Coupled Cavity Filter

Jingchao Wang, Rui Wang *, Lezhong Li, Junlin Guo and Jian Zhang

College of Optoelectronic Engineering, Chengdu University of Information Technology, Chengdu 610025, China

* Correspondence: rfywr@cuit.edu.cn

Abstract: This paper presents a new design method for a capacitor-loaded cross-coupled cavity filter, which significantly increases the power capacity of the cavity filter while improving out-of-band rejection. The filter uses a coaxial resonator at the open end of the donut capacitive-load. A triangular form of cavity structure is used for the full-cavity arrangement to reduce the size of the filter. In order to validate the design, a filter with a center frequency of 2.08 GHz and bandwidth of 80 MHz was designed, processed, and tested. The measured insertion loss was ≤ 0.97 dB, and the return loss was >20 dB in the range of 2040 MHz to 2120 MHz; the rejection was as high as 80 dB, and in-band ripple was 0.06 dB in the upper and lower stopband-range, which was only 30 MHz away from the sideband. After a simulation of the model using HFSS software (HFSS 2021, Canonsburg, PA, USA), the measured results matched the simulation results, which verified the correctness and practicality of the design. Compared with the ordinary-disc-load resonant cavity, the new donut capacitively loaded cavity-bandpass-filter has a 13.2% reduction in height and a 29.7% increase in power capacity.

Keywords: cavity filter; new capacitive load; cross coupling; coaxial resonator; power capacity

1. Introduction

Microwave filters are integral to wireless communication systems, allowing the desired signal to pass through while the unwanted signal is suppressed. Communication systems have to use bandpass filters to control the size of the loss, in order to transmit with the lowest possible loss, especially in RF circuits. In recent years, with the rapid development of communication technology, the use of high-frequency-band electromagnetic waves more and more frequently will inevitably lead to the increasing tension of spectrum resources and more stringent requirements for performance parameters. Coaxial-cavity bandpass filters have been widely used in communication base stations, satellite navigation, military radar and other fields, due to their low insertion-loss, high band-rejection and high selectivity [1–6]. In the field of RF microwaves for coaxial-cavity filters, many studies have been carried out by previous scholars, at home and abroad. The literature [7] designed a comb coaxial cavity filter using conventional spatial coupling, but the drawback is that the in-band insertion loss is not good enough. On this basis, the introduction of dielectric coaxial cavity makes the performance of the literature [8] improved; however, its volume still needs to be improved. A four-cavity cascaded cavity filter for the LTE band based on a stepped-impedance coaxial cavity was proposed in the literature [9], to solve this problem. However, the development of communication technology has put new requirements on the out-of-band rejection of the filter and the filter unloaded Q. In this context, cross-coupled structures capable of generating transmission zeros out-of-band in order to be able to improve frequency selectivity have been created [10–12]. In addition, the filter size reduction is inevitably accompanied by a reduction of the cavity power capacity. Therefore, it is crucial to consider the power capacity [13–15].

Based on the above analysis, first, by introducing a new capacitive-load coupling disc shaped like a doughnut and loaded onto the top of the metal coaxial resonator, the load capacitance is increased, and the maximum breakdown electric field of the resonator is also increased. Second, a generalized Chebyshev filter is designed and processed, and the cavity



Citation: Wang, J.; Wang, R.; Li, L.; Guo, J.; Zhang, J. Design of a New Capacitive Load Cross-Coupled Cavity Filter. *Electronics* **2023**, *12*, 142. <https://doi.org/10.3390/electronics12010142>

Academic Editor: Giovanni Crupi

Received: 17 November 2022

Revised: 17 December 2022

Accepted: 20 December 2022

Published: 28 December 2022



Copyright: © 2022 by the authors. Licensee MDPI, Basel, Switzerland. This article is an open access article distributed under the terms and conditions of the Creative Commons Attribution (CC BY) license (<https://creativecommons.org/licenses/by/4.0/>).

and resonator are arranged in a “triangular” fashion, to reduce the cavity size effectively. Third, the cavity-filter power capacity is analyzed at the theoretical level, and the power capacity values are calculated separately. Finally, the measured results are presented.

2. Novel Capacitive-Load Metal Resonator

The cavity height of a single resonant cavity is generally slightly more significant than the internal coaxial-resonator height. For the traditional quarter-wavelength “water-pipe type” coaxial resonant cavity, the bottom short-circuit end is equivalent to the total inductance. In contrast, the open end of the top water-pipe conductor is equivalent to the total capacitance. However, this structure has an extended resonator height, the resonant frequency is not well tuned, and there are other problems. The equivalent model is shown in Figure 1.



Figure 1. Equivalent model of quarter-wavelength coaxial resonant cavity.

In order to solve such problems, a novel capacitive-load-coupling disc with the shape of a “doughnut” is loaded on the open end of the inner conductor. According to the parallel-plate capacitance-effect Equation (1), the size of the equivalent capacitance of the top of the resonator is proportional to the area of the disc. The larger the area, the larger the equivalent capacitance at the top:

$$C = \frac{\epsilon_r \epsilon_0 S}{4\pi k d} \quad (1)$$

From Equation (2), it is easy to see that the magnitude of the equivalent capacitance at the top will affect the height, l , of the resonator:

$$\frac{\cot(\beta l)}{Z_0} - \omega_0 C = 0 \quad (2)$$

Equation (3), which is transformed from Equation (2), clearly states that “the larger the equivalent capacitance, the smaller the height of the resonator”:

$$l = \frac{\arctan(1/Z_0 \omega_0 C)}{\beta} = \frac{\lambda}{2\pi} \arctan\left(\frac{1}{Z_0 \omega_0 C}\right) \quad (3)$$

Since $0 < \arctan(1/Z_0 \omega_0 C) < \pi/2$, so $0 < l < \lambda_0/4$, that is, the presence of a concentrated capacitance will make the height of the resonant cavity shorter than that of a quarter-wavelength coaxial resonant cavity without the capacitance, and the larger the C , the shorter the l . Therefore, this capacitance is called “shortening capacitance”.

From Figure 2a–c, the impact of the capacitive loading method is vividly illustrated. After loading the standard disc, the capacitive effect at the top of the resonator is enhanced, and the resonator height is reduced. After replacing the standard disc with the donut load-disc, the length in the vertical direction decreases further, which is why this paper chooses Figure 2c. Therefore, a new capacitive-load-coupling disc with a larger area and a circular treatment is used to replace the traditional water-pipe type and standard discs. The larger disc area and the “swirl” depression of the disc-opening increases the top equivalent capacitance and shortens the resonant cavity’s length, thus achieving miniaturization.

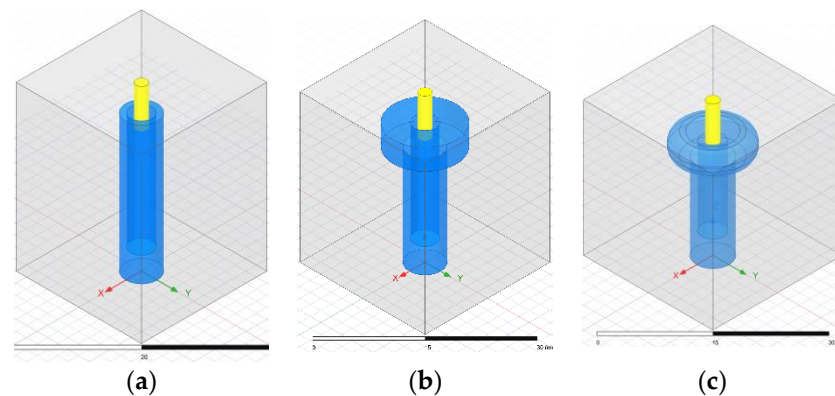


Figure 2. Schematic diagram of (a) water-pipe-type coaxial resonant (b) standard-disc coaxial resonant (c) donut capacitor-loaded coaxial resonant.

In addition, since the resonant cavity height is closely related to the resonant frequency, the resonant frequency of the resonant cavity changes, while the equivalent capacitance changes. From Table 1, the larger the effective contact area of the load, the lower the resonant frequency of the resonant. If the standard disc resonant in Figure 2b is used, the single cavity size is $24 \times 24 \times 28.3 \text{ mm}^3$, and the resonant frequency is 2213.4 MHz. However, suppose the new capacitor-loaded resonant of the donut is used. In that case, the resonant rod diameter is 6 mm, the single-resonant cavity size becomes $24 \times 24 \times 25 \text{ mm}^3$, and the resonant frequency reaches 2.102 GHz. Thus, it can be seen that using the new capacitively loaded resonant not only reduces the center frequency of the resonant but also reduces the height of the resonant by 13.2%. Therefore, we can use the “donut” load resonant to miniaturize the cavity filter.

Table 1. Relationship between loading mode and resonant frequency.

Type of Capacity Load	Direct	Disc	Donut
Resonant Frequency f (MHz)	2350.0	2213.4	2102.0

3. Design Principle of Cavity Filter

In this paper, an eighth-order two-zero-point cross-coupled coaxial cavity filter is designed using a donut capacitor-loaded metal resonator. The cavity filter is designed based on a generalized Chebyshev low-pass prototype filter, which produces an equal ripple response in the passband and has good rejection characteristics in the stopband. The design steps are divided into four main parts. First, the cavity-filter design starts with the index evaluation: Equation (4) is the filter transfer function:

$$|S_{21}(j\Omega)| = \frac{1}{1 + \epsilon^2 F_n^2(\Omega)} \tag{4}$$

In addition, the filter order is calculated by Equation (5), where Ω_s is the normalized frequency, L_{A_s} is the stopband rejection, and L_{A_r} is the in-band ripple:

$$n \geq \frac{\cosh^{-1} \sqrt{\frac{10^{0.1L_{A_s}} - 1}{10^{0.1L_{A_r}} - 1}}}{\cosh^{-1} \Omega_s} \tag{5}$$

Analyzing the filter topology is particularly important in the process of metrics evaluation. Different topologies correspond to completely different numbers and structures of transmission zeros, and therefore the performance of the designed filters varies greatly. According to the theoretical literature related to the design of transmission zeros for generalized Chebyshev filters [16–20], two couplings with different polarities are introduced:

cross-electric coupling and cross-magnetic coupling. By introducing cross-coupling, two transmission zeros outside the upper and lower passband, respectively, can be obtained, which helps to improve the out-of-band rejection. The filter topology of this design is shown in Figure 3.

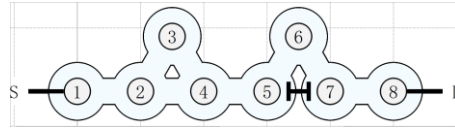


Figure 3. Cascaded triple topology.

After the topology is selected, the next step is to calculate the parameters of the coupling structure by using Equation (6) to calculate the inter-cavity coupling coefficient, where g_1 and g_2 is the normalized low-pass prototype value and FBW is the relative bandwidth:

$$k_{ij} = m_{ij} \times FBW = FBW / \sqrt{g_1 g_2} \tag{6}$$

Equation (7) is used to calculate the external Q of the cavity filter, and the external Q can be used to simulate the input–output coupling structure:

$$Q_L = 1 / (M_{S1} \times FBW) \tag{7}$$

In order to make the following simulation results more accurate, the circuit design software ADS (ADS2020, Santa Rosa, CA, USA) is used to extract the required network parameters. The filter group delay can be derived as 8.14 ns, and the two transmission zeros are 2010 MHz and 2150 MHz, respectively; the coupling matrix of the filter is shown in Figure 4.

0.00017	0.81932	0	0	0	0	0	0
0.81932	0.00019	0.55035	0.20996	0	0	0	0
0	0.55035	-0.39127	0.51105	0	0	0	0
0	0.20996	0.51105	0.01098	0.54379	0	0	0
0	0	0	0	-0.01002	0.51335	-0.20413	0
0	0	0	0	0.51335	0.38093	0.55255	0
0	0	0	0	-0.20413	0.55255	0.00019	0.81931
0	0	0	0	0	0	0.81931	0.00017

Figure 4. Coupling matrix of 2080 MHz bandpass filter.

Second, the simulation of the single-cavity and double-cavity coupling coefficients is based on the finalization of the index parameters. For single-cavity resonators, the ratio of the base half-length to the resonant rod radius is usually chosen to be between 4 and 7.2, to take into account the requirements of low loss and high power-capacity. In accordance with the above analysis, the base half-length, $p = 10$ mm, and the outer rod radius, $q = 3$ mm, are chosen in this paper. After determining the physical dimensions of the resonator to be $24 \times 24 \times 25$ mm³, the single resonant cavity was simulated in Ansys HFSS (HFSS 2021, Canonsburg, PA, USA), scanning the length of the tuning screw inserted into the cavity to determine the model to operate at the center frequency. The resonant frequency, f , of the donut’s new capacitively loaded metal resonator is given in Figure 5 as a function of the screw length, t .

Third, the dual-cavity coupling coefficient simulation is determined using the “dual-mode extraction method”. The two modes are set in HFSS using the eigenmode solver, and the width of the middle air window is scanned with Equation (8), which corresponds to the coupling coefficient calculated in the index evaluation stage. For the simulation

of the external Q value, the center height of the input and output taps was simulated to correspond to the group-time-delay value of 8.14 ns:

$$k_{ij} = \frac{f_1^2 - f_2^2}{f_1^2 + f_2^2} \tag{8}$$

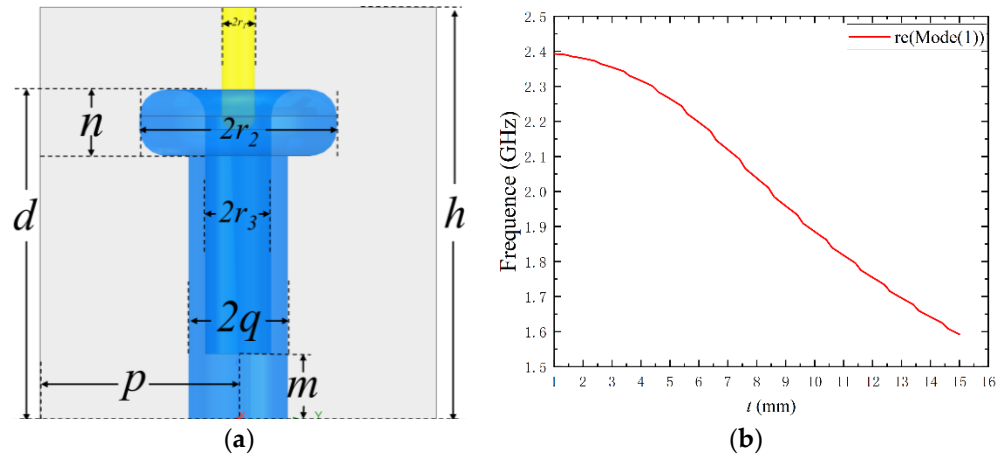


Figure 5. Schematic diagram of (a) donut capacitor-loaded resonator (b) single-cavity resonance frequency variation with screw length. (Initial dimensions in mm: $d = 20, h = 25, m = 4, n = 4, p = 12, q = 3, r_1 = 1, r_2 = 6, r_3 = 2$).

Fourth, Figure 6 shows the overall structure of the proposed eighth-order compact cavity filter, which can effectively reduce the filter size through the cavity and resonator “Z-shaped” topology.

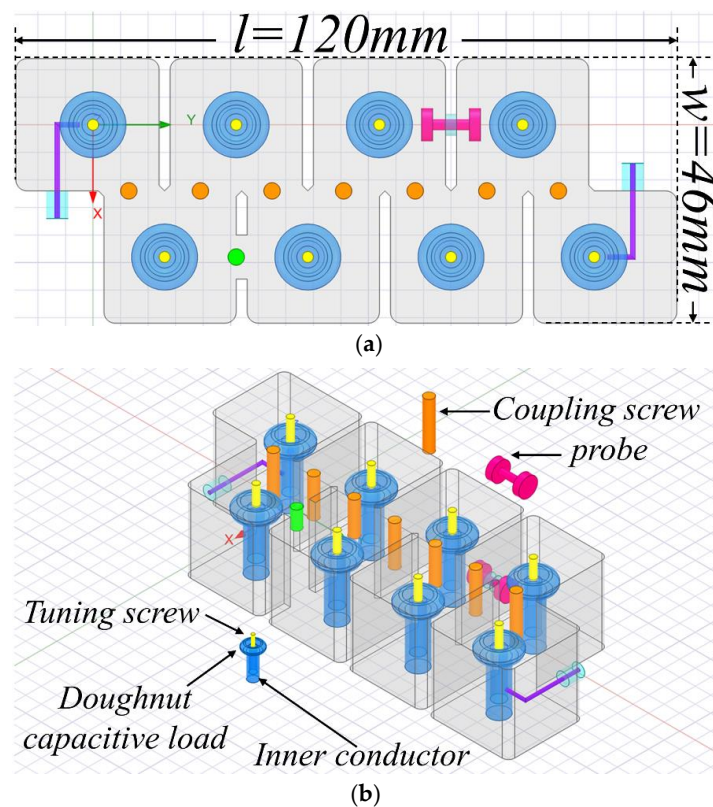


Figure 6. Schematic diagram of (a) Cavity filter layout (top) and (b) its photograph (3D view).

The direct coupling as the primary path is from 1 to 8 in sequence, while the cross-coupling as the auxiliary path is between 2 and 4 and 5 and 7.

After joint simulation and optimization using the ADS and HFSS software, the S-parameter frequency response is obtained, as shown in Figure 7, where the return loss is ≥ 20 dB in the passband range of 2.04 to 2.12 GHz. Due to the introduction of two transmission zeros outside the band, the rejection characteristics are good, and possess 36 dB rejection in the stopband range, leaving the sideband of 0.02 GHz.

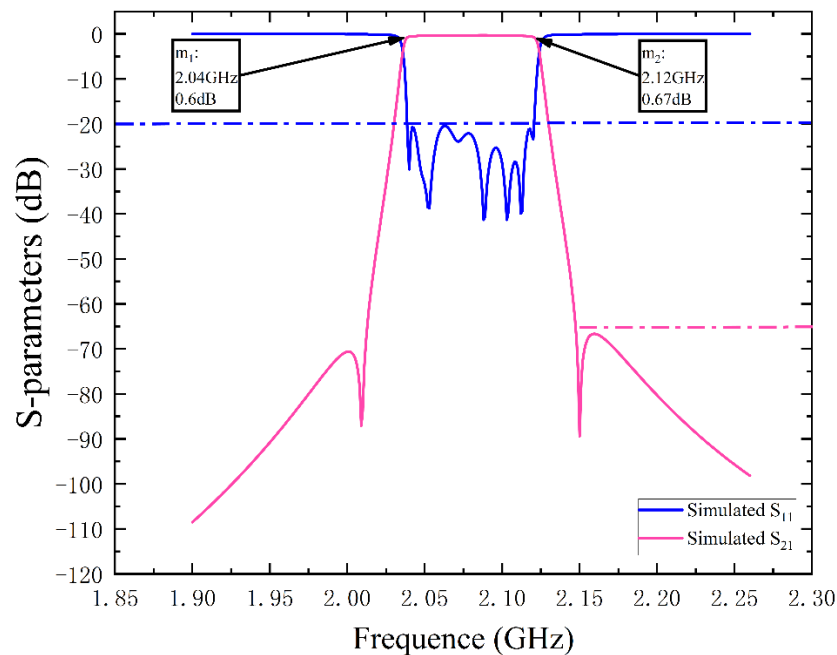


Figure 7. Frequency response of 2080 MHz simulation model.

4. Analysis of Power and Filter Simulation Results

Different cavity structures will lead to differences in the electromagnetic field distribution. The electric field distribution of a single cavity with a fixed resonator is expressed as Equation (9):

$$\vec{E} = E_{\max} \cdot \vec{f}(x, y, z) \tag{9}$$

The resonant cavity electric-energy storage is expressed as Equation (10), where E_{\max} is the electric field amplitude at the point of maximum field strength, and $f(x, y, z)$ is the electric field’s distribution function, characterizing the distribution’s specific situation; its modulus value is maximum 1, that is, $|f(x, y, z)| = 1$:

$$W_e = \int_V \epsilon |E|^2 dV \tag{10}$$

The magnitude of cavity excitation-power will change the maximum point of field strength, and the distribution function $f(x, y, z)$ is independent of the cavity excitation-power. The total energy-storage size in a single cavity can be obtained from the above two equations, as shown in Equation (11):

$$W_{\max} = \frac{\epsilon_0}{2} \int_V \vec{E} * \vec{E}^* dV = E_{\max}^2 \left(\frac{\epsilon_0}{2} \int_V \vec{f}(x, y, z) \cdot \vec{f}^*(x, y, z) dV \right) = \frac{1}{\zeta^2} E_{\max}^2 \tag{11}$$

After the single cavity is determined, as shown in Equation (12), if the maximum field strength is divided by the quadratic root of the total stored energy, we will find that ζ is constant, which indicates that the amplitude squared of the maximum electric field

is linearly related to the total stored energy. Furthermore, Equation (13) can be used to calculate the scale factor between the cavity input-power and the maximum stored-energy:

$$\zeta = \frac{E_{\max}}{\sqrt{W_{\max}}} = \frac{1}{\sqrt{\frac{\epsilon_0}{2} \int_V \vec{f}(x, y, z) \cdot \vec{f}^*(x, y, z) dV}} \tag{12}$$

$$\eta = W_{\max} / P_{in} \tag{13}$$

Combining the two equations above, the relationship between the filter-port input power and breakdown field-strength can be derived as Equation (14):

$$E_{\max} = \zeta \sqrt{\eta P_{in}} \tag{14}$$

If the filter is to work safely, the maximum value of the field strength in the resonator must be less than the electric-field breakdown value of the air; otherwise, the filter will be broken down. When the two are equal in magnitude, the maximum value of the cavity power-capacity can be calculated using Equation (15). The breakdown field-strength of air at regular atmospheric pressure can be taken as $E_p = 2.9 \times 10^6$ V/m, and the maximum energy storage of a single cavity calculated using CST Filter 3D software (CST Studio Suite 2022, Darmstadt, Germany) is 3.07173×10^{-8} J:

$$P_{\max} = \frac{1}{\eta} \left(\frac{E_p}{\zeta} \right)^2 \tag{15}$$

The above cavity power-capacity theory [21,22] is integrated, and the electric field distribution of the two resonators is solved separately, based on two different resonator structures using the simulation software HFSS, while the power capacity is calculated for comparison. From the single-cavity electric-field distribution plot in Figure 8, the maximum field strength $\zeta_1 = 3.8841 \times 10^9$ V/m, $\zeta_2 = 3.4415 \times 10^9$ V/m, $\zeta_3 = 2.9960 \times 10^9$ V/m at a single-cavity energy storage of 1 Joule can be calculated by the intrinsic imitation of the truth, with the guarantee that the resonant frequencies are all at 2080 MHz. Therefore, in accordance with the cavity-filter-power-capacity calculation in Equation (11), the power capacity magnitudes of the three resonators can be obtained as 18.15 W, 23.52 W, and 30.5 W, respectively. This shows that the power capacity of the donut capacitor-loaded resonator increases by $(30.5 - 23.52) / 23.52 \times 100\% = 29.7\%$, compared with the standard-disc-loaded resonator.

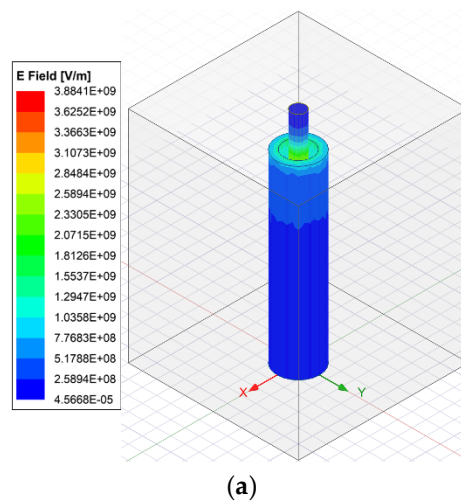


Figure 8. Cont.

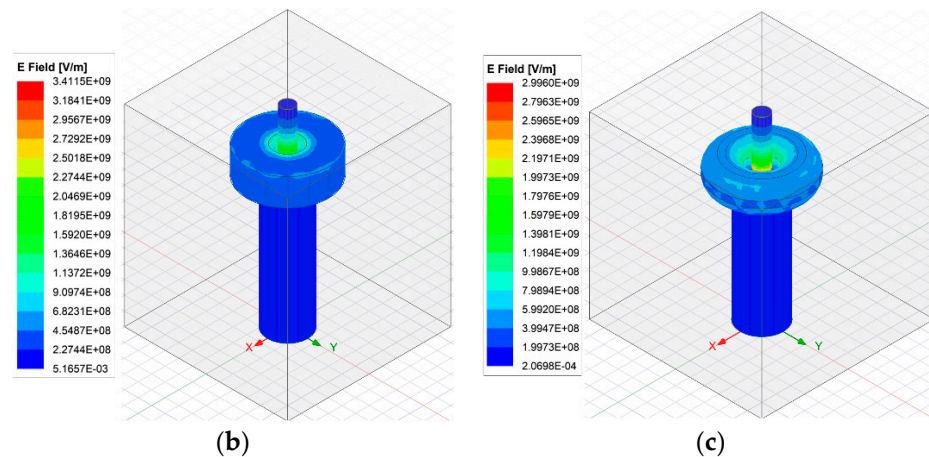


Figure 8. Single-cavity electric field model of (a) water-pipe-type coaxial resonant (b) standard-disc coaxial resonant (c) donut capacitor-loaded coaxial resonant.

5. Processing and Testing Results

A new 2080 MHz capacitively loaded bandpass filter was machined and tested, to verify the design. Figure 9 shows a physical photo of the machined bandpass filter, and Figure 10 measured response of a new 2080 MHz capacitively loaded cavity-filter, processed.



Figure 9. Physical view of the new 2080 MHz capacitive-load cavity-filter processed.

Figure 10 shows the measurement of the filter-scattering parameters, using a vector network analyzer, Agilent E8358A.

Considering that the loss caused by the cable between the VNA and DUT (CL bandpass filter) has some influence on the test, a two-port SOLT (short open load and straight-through) calibration was performed. Figure 10 shows that the filter measures the passband from 2.04 GHz to 2.12 GHz, with return loss substantially better than 20 dB over almost the entire passband. In addition, an insertion loss of 0.91 dB and 0.97 dB is measured at 2010 MHz and 2150 MHz, respectively. Out-of-band rejection of 88 dB is achieved in a range only 100 MHz from the upper sideband. The agreement between the measured and simulated results is good. However, there is still some deviation during the actual measurement. Factors may cause this slight difference. For example, the SMA connector has certain losses during the assembly process, aggravating the fluctuation of in-band insertion loss. In addition, mechanical errors in milling machine processing may lead to differences in resonant cavity dimensions, thus affecting the unloaded Q of the filter. However, in general, these errors are within the error tolerance.

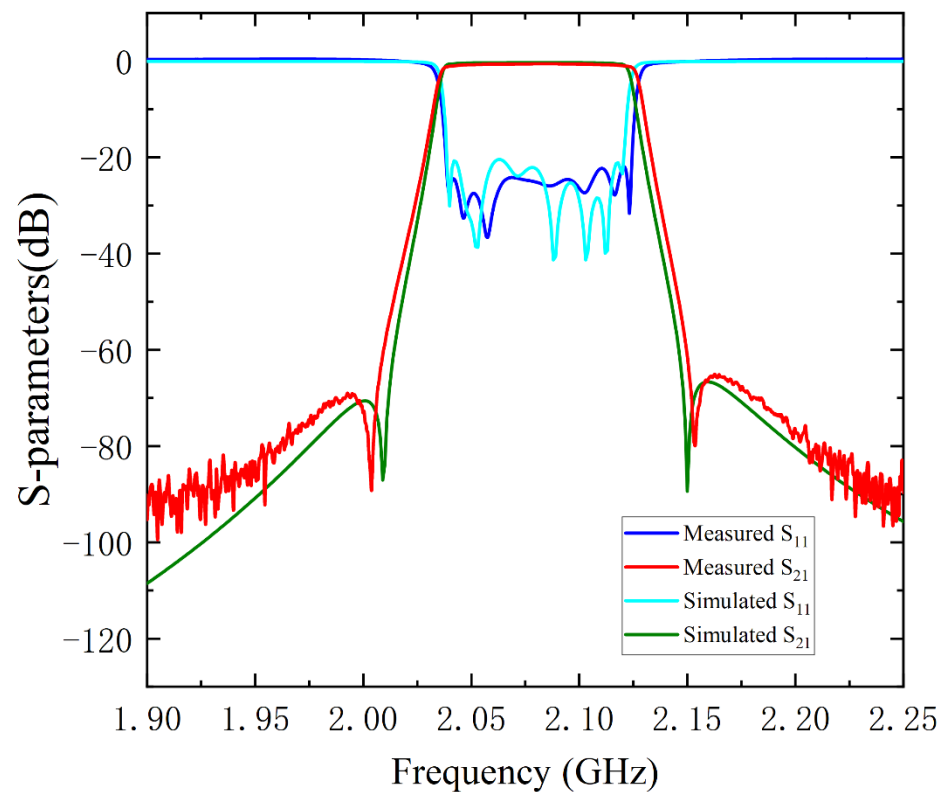


Figure 10. Measured response of a new 2080 MHz capacitively loaded cavity-filter, processed.

To check the performance of the proposed and processed filter, Table 2 compares it with several recent CL filters for parameters such as out-of-band rejection.

Table 2. Comparison of the proposed-filter performances with related published works.

Ref.	f_0 (GHz)	BW (GHz)	IL (dB)	RL (dB)	Q	Size (λ_g^2)	Resonator Type
[17]	1.54	0.040	1.45	20	3000	0.87×0.67	Cavity
[18]	37.24	0.56	1.3	17	3365	4.88×2.1	Waveguide
[19]	4.0	0.25	2.48	17	260	1.4×0.28	SIW
[20]	4.5	0.2	1.5	15	2500	0.7×0.53	Cavity
This work	2.08	0.08	0.97	45	4677	0.84×0.32	Cavity

6. Conclusions

This paper proposes a novel capacitive-load cross-coupled cavity bandpass-filter with high stopband rejection, miniaturized size and higher power-capacity. The power capacity of the cavity is further enhanced by using a new resonator loaded with a donut disc to improve on the traditional plumbing-type coaxial resonator. The power capacity that the cavity can withstand is further improved by using a new resonator loaded with a donut disc, to modify the conventional water-pipe-type coaxial resonator. Then, two out-of-band transmission zeros are formed by introducing inductive–capacitive coupling, which significantly improves the signal rejection outside the filter passband. The measured total length has a center frequency of 2.08 GHz, a bandwidth of 80 MHz, a VSWR of less than 1.22, and a stopband rejection of greater than 80 dB at 2010 MHz and 2150 MHz. The measured results agree with the simulated results, verifying the feasibility and practicality of the new capacitive-load resonator miniaturization method. Overall, the filter has the advantages of miniaturization, significant stopband rejection, and good selectivity. Therefore, the pro-

posed filter with improved performance makes it suitable for a wide range of applications, such as base stations and satellites.

Author Contributions: Conceptualization, J.W.; methodology, J.W.; software, J.W.; validation, J.Z. and J.G.; formal analysis, R.W.; investigation, J.Z.; resources, J.W.; data curation, J.W.; writing—original draft preparation, J.W.; writing—review and editing, J.W., R.W. and L.L.; visualization, J.W.; supervision, R.W. and L.L.; project administration, J.Z. and J.G.; funding acquisition, L.L. All authors have read and agreed to the published version of the manuscript.

Funding: Funding was provided by the Natural Science Foundation of Sichuan Province, (Grant No. 2022NSFSC0524), Transfer Payment Project of Sichuan Province under Grant nos, (Grant No. R21ZYZF0001).

Data Availability Statement: Please refer to suggested Data.

Conflicts of Interest: The authors declare no conflict of interest.

References

- Laplanche, E.; Delhote, N.; Périgaud, A.; Tantot, O.; Verdeyme, S.; Bila, S.; Pacaud, D.; Carpentier, L. Tunable Filtering Devices in Satellite Payloads: A Review of Recent Advanced Fabrication Technologies and Designs of Tunable Cavity Filters and Multiplexers Using Mechanical Actuation. *IEEE Microw. Mag.* **2020**, *21*, 69–83. [\[CrossRef\]](#)
- Rong, C.; Xu, Y.; Xia, M.; Luo, Y.; Ou, R. Broadband class E GaN power amplifier design in S band with low-pass match. In Proceedings of the 2014 IEEE International Conference on Communication Problem-Solving, Beijing, China, 5–7 December 2014; pp. 372–375.
- Maity, S.; Ghosal, R.; Gupta, B. Modal Charts of Cylindrical Dielectric Resonators [Application Notes]. *IEEE Microw. Mag.* **2021**, *23*, 54–71. [\[CrossRef\]](#)
- Shahid, I.; Thalakituna, D.; Karmokar, D.K.; Mahon, S.J.; Heimlich, M. Periodic Structures for Reconfigurable Filter Design: A Comprehensive Review. *IEEE Microw. Mag.* **2021**, *22*, 38–51. [\[CrossRef\]](#)
- Doumanis, E.; Goussetis, G.; Vuorio, J.; Hautio, K.; Amper, O.; Kuusmik, E.; Pallonen, J. Tunable Filters for Agile 5G New Radio Base Transceiver Stations [Application Notes]. *IEEE Microw. Mag.* **2021**, *22*, 26–37. [\[CrossRef\]](#)
- Mao, C.X.; Zhang, Y.; Zhang, X.Y.; Xiao, P.; Wang, Y.; Gao, S. Filtering Antennas: Design Methods and Recent Developments. *IEEE Microw. Mag.* **2021**, *22*, 52–63. [\[CrossRef\]](#)
- Anwar, M.S.; Dhanyal, H.R. Design of S-band combline coaxial cavity bandpass filter. In Proceedings of the 15th International Bhurban Conference on Applied Sciences and Technology (IBCAST), Islamabad, Pakistan, 9–13 January 2018; pp. 866–869.
- Zhongxiang, Z.; Chang, C.; Xianliang, W. A compact cavity filter with novel TM mode dielectric resonator structure. In Proceedings of the IEEE International Conference on Microwave Technology & Computational Electromagnetics, Beijing, China, 22–25 May 2011; pp. 111–113.
- In, J.H.; Kim, M.; Kim, H.; Yang, Y. A cavity filter using stepped impedance coupling resonator. In Proceedings of the 12th International Conference on Advanced Communication Technology (ICACT), PyeongChang, Korea, 7–10 February 2010; pp. 436–439.
- Li, S.; Wang, X.; Li, Y.; Wang, J. Design of Compact Coaxial Cavity Bandpass Filter with High Selectivity. In Proceedings of the IEEE MTT-S International Microwave Biomedical Conference (IMBioC), Nanjing, China, 6–8 May 2019; pp. 1–4.
- Yu, Y.P.; Li, Y.F. Design of a small size C-band cavity bandpass filter. In Proceedings of the IEEE USNC-URSI Radio Science Meeting (Joint with AP-S Symposium), Marina Bay Sands, Singapore, 4–10 December 2021; pp. 86–87.
- Zhang, Z.; Ding, J.; Wang, S.; Zhang, H. Design of Asymmetric Dual-Band Microwave Filters. *Prog. Electromagn. Res. Lett.* **2017**, *67*, 47–51. [\[CrossRef\]](#)
- Rong, C.; Xu, Y.; Zhang, Y. Dielectric-Loaded Miniaturized Cavity Bandpass Filter with Improved Power Capacity. *Electronics* **2022**, *11*, 1441. [\[CrossRef\]](#)
- Vallerotonda, P.; Cacciamani, F.; Pelliccia, L.; Cazzorla, A.; Tiradossi, D.; Steffè, W.; Vitulli, F.; Picchione, E.; Galdeano, J.; Martín-Iglesias, P.; et al. Dielectric-loaded L-band filters for high-power space applications. *Int. J. Microw. Wirel. Technol.* **2022**, *14*, 282–292. [\[CrossRef\]](#)
- Psychogiou, D.; Ashley, A. Glass-Based Bandpass Filters for New Radio (NR) K/Ka-band Communications. *IEEE Trans. Compon. Packag. Manuf. Technol.* **2022**, *12*, 887–889. [\[CrossRef\]](#)
- Thomas, J.B. Cross-coupling in coaxial cavity filters—a tutorial overview. *IEEE Trans. Microw. Theory Techn.* **2003**, *51*, 1368–1376. [\[CrossRef\]](#)
- Vallerotonda, P.; Cacciamani, F.; Pelliccia, L.; Aquino, F.; Tomassoni, C.; Martín-Iglesias, P.; di Crestvolant, V.T. Dielectric-loaded Ku-Band Filter for High-power Space Applications based on Barrel-shaped cavities. In Proceedings of the 2021 51st European Microwave Conference (EuMC), London, UK, 4–6 April 2022; pp. 35–38.
- Alós, E.A.; Zaman, A.U.; Kildal, P.S. Ka-Band Gap Waveguide Coupled-Resonator Filter for Radio Link Diplexer Application. *IEEE Trans. Compon. Packag. Manuf. Technol.* **2013**, *3*, 870–879. [\[CrossRef\]](#)

19. Le Coq, M.; Rius, E.; Favennec, J.F.; Quendo, C.; Potelon, B.; Estagerie, L.; Moroni, P.; Bonnet, B.; Mostrah, A.E. Miniaturized C-Band SIW filters using high-permittivity ceramic substrates. *IEEE Trans. Compon. Packag. Manuf. Technol.* **2015**, *5*, 620–626. [[CrossRef](#)]
20. Soi, S.; Singh, S.K.; Singh, R.; Kumar, A. C-Band Iris Coupled Cavity Bandpass Filter. In Proceedings of the IEEE International Conference on Signal Processing and Communications (SPCOM), Bangalore, India, 11–15 July 2022; pp. 1–5.
21. Huong, T.T.T.; Do Tuan, A.; Thao, T.T.; Vu, V.Y. Novel Resonator Structure to Improve Power Handling Capacity in Iris Coupled Cavity Filter. In Proceedings of the 2019 International Conference on Advanced Technologies for Communications (ATC), Hanoi, Vietnam, 17–19 October 2019; pp. 98–102.
22. Li, Z.R.; Xu, G.; Zeng, R.; Lv, L.M.; Li, W.J.; Li, X.H. Failure Analysis of Microwave Air Breakdown for the Cavity Filter with Remainder. In Proceedings of the 48th European Microwave Conference (EuMC), Madrid, Spain, 23–27 September 2018; pp. 97–100.

Disclaimer/Publisher’s Note: The statements, opinions and data contained in all publications are solely those of the individual author(s) and contributor(s) and not of MDPI and/or the editor(s). MDPI and/or the editor(s) disclaim responsibility for any injury to people or property resulting from any ideas, methods, instructions or products referred to in the content.